Proceedings of ASME Turbo Expo 2011
GT2011
June 6-10, 2011, Vancouver, British Columbia, Canada

GT2011-46030

NUMERICAL INVESTIGATION AND PERFORMANCE OPTIMIZATION OF AN AIR-COOLED STEAM CONDENSER CELL UNDER AMBIENT CONDITIONS

Weifeng He
Institute of Turbomachinery,
Xi'an Jiaotong University
Xi'an, Shaanxi, China

Yiping Dai*
Institute of Turbomachinery,
Xi'an Jiaotong University
Xi'an, Shaanxi, China

Qingzhong Ma
Shanxi Electric Power Research Institute
Taiyuan, Shanxi, China

ABSTRACT

Air-cooled steam condensers (ACSCs) are so sensitive to the unpredictable ambient conditions that it is quite necessary to find the mechanism how the ambient conditions get into reaction and reasonable measurements can be employed to improve the performance. The numerical model of an ACSC cell is established in the paper. The influence of the ambient conditions on the performance of the ACSC cell is investigated, and the final stable back pressure (absolute pressure) the ACSC cell operates at is forecasted. Finally, wind wall is equipped to change the flow field around the ACSC cell and the performance is optimized.

Aerodynamic characteristic of the ACSC cell is simulated by employing the FAN boundary and porous media model in FLUENT. User Define Function (UDF) based on the actual steam property is loaded to simulate the condensation of the steam in the exchangers.

The flow field around the ACSC cell varies with the different wind speeds and directions. As a result, the fan volumetric effectiveness and the exchanger performance both decrease under high wind speed and adverse wind direction. Wind temperature gets into reaction mainly because it changes the cold side temperature of the exchangers. Under high wind temperature, the reduced temperature difference decreases the heat transfer rate between the exhaust steam and the ambient air. The equipped wind wall successfully reduces the hot air recirculation (HAR) although the fan performance is also affected due to the gathering effect between the wind wall and heat exchangers, and the performance of the ACSC cell is significantly improved under the dual effects.

1. INTRODUCTION

ASCSs have been utilized in many fields such as power industry. It is very adaptive for the place which is short of water resource because the Rankine cycle in the direct air-cooled power plant is completely closed and it is not necessary to exchange recycled water during operation periods. This pattern of station has been vigorously popularized recently since the water problem becomes serious.

ACSCs are exposed to the environment, and the windy conditions will influence the flow field around the ACSC. As a result, performance of the axial fans and heat exchangers will also be affected. Air flow reduction of the air-cooled heat exchangers having different numbers of fan rows under the effect of the flow disturbances and distortions were investigated experimentally by Salta [1]. Stinnes [2] studied the effect of cross-flow and off-axis inflow on the performance of air-cooled fans. The numerical research by P.J. Hotchkiss [3] confirmed the findings of Stinnes. A numerical model based on the blade element theory which is applied to simulate the flow-field near an axial flow fan was proposed [4, 5], and the effect of inlet flow distortions on the air-cooled heat exchanger performance was numerically simulated with the help of the model [6-9]. Meyer [10, 11] experimentally investigated the flow loss of different heat exchangers since the exchanger characteristic influences the ACSC volumetric effectiveness.

* Professor and author of correspondence

The quantitative analysis on the performance of the ACSC has been investigated. Effect of the wind speed, direction and height of the air-cooled platform on the ASCS performance was numerically simulated [12]. The simplified model with a cubic fluid zone is considered to be the ACSC cell, and all the results are based on the assumption. It was found that the ACSC performance decreases with the increase of wind speed and increases as the platform height is elevated. In addition, the performance increased rapidly with the increase of the wind direction angle up to a critical value, and then leveled off. Van Rooyen [13] found that the flow distortions and corresponding low-pressure region at the upstream edge fans mainly contribute to the net decrease of the ASCS performance as the wind speed increases, but the wind does have a positive influence on certain fans. M.T.F. Owen [14] studied the effect of screens on the ACSC performance under windy conditions, and it was found that the existing wind screen configuration raises the ACSC performance under windy conditions relative to the no screens case.

Hot air recirculation is always emphasized because the phenomenon will result in performance reduction of the ACSC. Gu *et al.* [15] discussed the wind tunnel criteria for simulating HAR in an ACSC and described the experimental methods. Both the wind speed and the height of the ACSC platform affect the recirculation, and the wind direction has a significant effect on the total recirculation, as well as its distribution across the inlets of an ACSC platform. Liu *et al.* [16] numerically proved the influence of the windy conditions on the HAR, and appropriate measures were advised to reduce the HAR such as the increment of the wind wall height and the fan rotational speed. But the fluid zone inside the A-frame is ignored, and the fan and exchanger surfaces are just considered to be boundaries.

Direct air-cooled power plants universally operate at a sub-stable status since the sensitivity of the ACSC to the windy conditions. It is necessary to investigate the flow field around the power plant under local meteorological conditions. Computational Fluid Dynamics (CFD) has been widely used to investigate the ACSC performance under windy conditions due to its great advantage compared to the experimental methods. It is significant to investigate the performance of the ACSC cell under the effect of the windy conditions because the influence principle of the cell performance is just the same to that of the whole ACSC, and the results is used to guide the design and operation of the ACSC. In the paper, a practical numerical model is proposed to simulate the flow field around the ACSC cell, and the principles how the windy conditions get into reaction on the cell performance is investigated. Heat transferring with phase transition is so complicated that User Define Function (UDF) is introduced to simulate the condensation of the exhaust steam in the fin-tube heat exchangers. Thus ACSC cell performance under windy conditions is numerically investigated, and the corresponding back pressure is forecasted through the comparison between the ideal heat release and the actual heat transfer rate. In addition, wind wall is equipped to reduce the HAR phenomenon, and ACSC cell performance under the effect of the wind wall is also calculated.

2. GEOMETRY AND FLUID MODEL

The geometric structure of the investigated ACSC cell, 45m above the ground, is presented in Fig. 1. The air-cooled A-frame mainly consists of an axial-flow fan, 9.144m in diameter, and single fin-tube heat exchangers, 10.7m×12.6m×0.22m. The wind tube is 2.1m in height. Turbine exhaust condensates in the exchangers while ambient air outside absorbs the latent heat the steam releases.

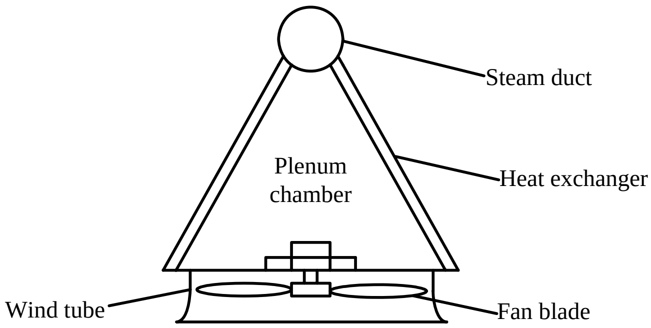

Fig. 1 Geometric structure of the ACSC cell

FAN boundary condition in FLUENT is applied to simulate the pressure jump when the air flows through the rotor. The fan surface located at the center of the wind tube, and the performance curve is fitted according to the supplied information by the fan manufacture:

$$\Delta p_f = 202.1 - 9.5 v_n - 0.8 {v_n}^2 \quad (1)$$

where Δp_f is the pressure rise; v_n is the normal velocity to the fan surface.

The mechanical energy loss resulting from the fin-tube exchangers (corresponding pressure drop) is taken into account by a viscous and an inertial loss with porous media model. The flow loss term added to Navier-Stokes equations can be defined [17]:

$$S = \frac{\mu}{\alpha} v_f + C \frac{1}{2} \rho {v_f}^2 \quad (2)$$

where μ is the dynamic viscosity; α is the permeability; ρ is the density; C is the inertial loss coefficient; v_f is the frontal velocity. In the paper, only the inertial loss is considered during the simulation, and the corresponding pressure drop is expressed [18]:

$$\Delta p_e = C \frac{1}{2} \rho {v_f}^2 \Delta n \quad (3)$$

where Δn is the thickness of the exchanger, Δn=0.22m. Experimental results on the exchanger resistance are employed to determine the coefficient, C=139.5.

Turbine exhaust condensates in the exchangers when the ambient air flows outside. It is very difficult to simulate the condensation directly because multiphase flow is involved in the process. The temperature, pressure, specific heat and other physic parameters of the steam are all variable during condensation. In addition, the calculation capacity will be tremendous. As a result, UDF based on the actual water and steam property is first applied to simulate the condensation of the steam in the fin-tube exchangers. The turbine exhaust turns to be saturated water at first and then subcools if possible in the UDF. The heat exchanger is considered to be fluid zone during the simulation, and heat release in each grid is obtained initially and then the sum of the grid release is just the total heat transfer rate between the ambient and the turbine exhaust.

Flow field around the ACSC cell is the core regions we emphasize, and these regions have a dense grid distribution in Fig. 2. The computational domain, 300m×300m×200m, contains about 3,280,000 grid elements in total, and the domain is divided into small parts to raise the grid quality. The maximum value of the equiangle skew is 0.64, and the maximum value of the aspect ratio is 3.1. The quality of the grid is fine enough to ensure the convergence and accuracy during simulation.

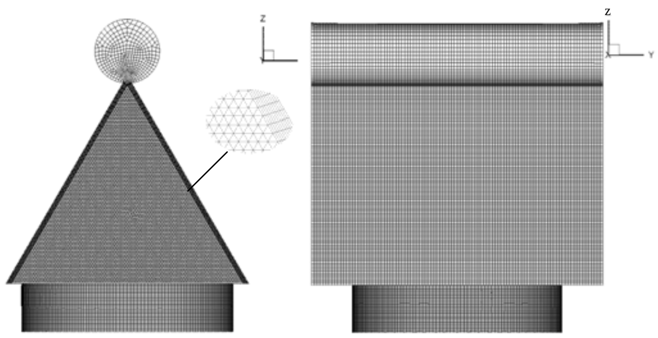

(a) Cross view of the mesh (b) Longitudinal view of the mesh

Fig. 2 Grid distribution around the ACSC cell

Heat transfer rate of the ACSC cell under three set of grids are calculated to verify the grid independence in Fig. 3. It can be inferred that the simulation result is reliable because the deviation among the three set grids is less than 1% although only the middle set, 3,280,000, is used in the investigation.

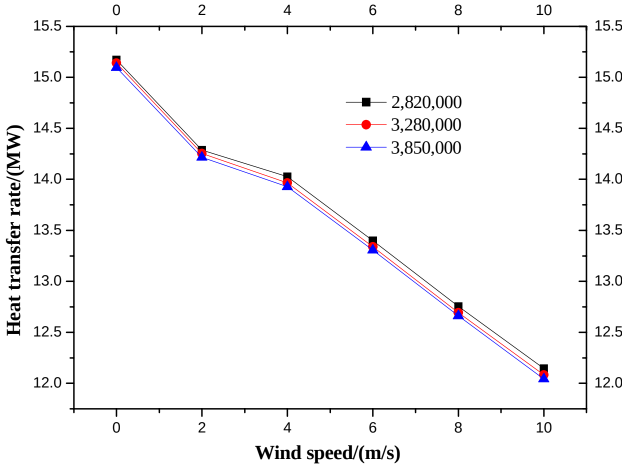

Fig. 3 Comparison of the heat transfer rate under three set grids

As a default, the SIMPLE solution algorithm is implemented in FLUENT, for a steady-state solution. Turbulence is modeled using the standard *k*-*ε* model. It is assumed that the flow is incompressible. Governing equations are the mathematical description of the conservation laws. The general governing equations are as follows:

$$\frac{\partial(\rho\phi)}{\partial t}+\frac{\partial(\rho v_x\phi)}{\partial x}+\frac{\partial(\rho v_y\phi)}{\partial y}+\frac{\partial(\rho u_z\phi)}{\partial z}=\frac{\partial}{\partial x}\left(\Gamma\frac{\partial\phi}{\partial x}\right)+\frac{\partial}{\partial y}\left(\Gamma\frac{\partial\phi}{\partial y}\right)+\frac{\partial}{\partial z}\left(\Gamma\frac{\partial\phi}{\partial z}\right)+S \quad (4)$$

where Φ stands for different variables, Γ is the corresponding generalized diffusion coefficient and S is the corresponding source term.

For the continuity equation:

$$\phi=1,\Gamma=0,S=0$$

For the momentum equation:

$$\left.\begin{aligned}
&x-direction\\
&\phi=v_x,\Gamma=\mu_{eff}=\mu+\mu_t,S=-\frac{\partial p}{\partial x}+\frac{\partial}{\partial x}\left(\mu_{eff}\frac{\partial v_x}{\partial x}\right)+\frac{\partial}{\partial y}\left(\mu_{eff}\frac{\partial v_y}{\partial x}\right)+\frac{\partial}{\partial z}\left(\mu_{eff}\frac{\partial v_z}{\partial x}\right)\\
&y-direction\\
&\phi=v_y,\Gamma=\mu_{eff}=\mu+\mu_t,S=-\frac{\partial p}{\partial y}+\frac{\partial}{\partial x}\left(\mu_{eff}\frac{\partial v_x}{\partial y}\right)+\frac{\partial}{\partial y}\left(\mu_{eff}\frac{\partial v_y}{\partial y}\right)+\frac{\partial}{\partial z}\left(\mu_{eff}\frac{\partial v_z}{\partial y}\right)\\
&z-direction\\
&\phi=v_z,\Gamma=\mu_{eff}=\mu+\mu_t,S=-\frac{\partial p}{\partial z}+\frac{\partial}{\partial x}\left(\mu_{eff}\frac{\partial v_x}{\partial z}\right)+\frac{\partial}{\partial y}\left(\mu_{eff}\frac{\partial v_y}{\partial z}\right)+\frac{\partial}{\partial z}\left(\mu_{eff}\frac{\partial v_z}{\partial z}\right)
\end{aligned}\right\}$$

For the energy equation:

$$\phi=T,\Gamma=\mu/P_r+\mu_t/\sigma_T$$

For *k* equation:

$$\phi=k,\Gamma=\mu+\mu_t/\sigma_k,S=G_k-\rho\varepsilon$$

For *ε* equation:

$$\phi=\varepsilon,\Gamma=\mu+\mu_t/\sigma_\varepsilon,S=\frac{\varepsilon}{k}\left(C_1G_k-C_2\rho\varepsilon\right)$$

where μ is viscosity, μ_t is turbulent viscosity, and μ_{eff} is effective turbulent viscosity.

$$\mu_t=\rho C_\mu\frac{k^2}{\varepsilon} \quad (5)$$

G_k is a term which generates because of turbulence kinetic energy *k* caused by the gradient of the average velocity.

$$G_k=\mu_t\left\{\begin{aligned}&2\left[\left(\frac{\partial v_x}{\partial x}\right)^2+\left(\frac{\partial v_y}{\partial y}\right)^2+\left(\frac{\partial v_z}{\partial z}\right)^2\right]+\left(\frac{\partial v_x}{\partial y}+\frac{\partial v_y}{\partial x}\right)^2\\&+\left(\frac{\partial v_x}{\partial z}+\frac{\partial v_z}{\partial x}\right)^2+\left(\frac{\partial v_y}{\partial z}+\frac{\partial v_z}{\partial y}\right)^2\end{aligned}\right\}$$

The Prantle number in the energy equation is taken as P_r=0.85. According to the recommended value, the empirical constants which appear in the turbulence equations are assigned the values shown in Table 1:

Table 1 Values of the constants in the turbulence equations

C_μ	C_1	C_2	σ_k	σ_ε
0.09	1.44	1.92	1.0	1.3

As shown in Fig. 4, the exponential wind speed distribution is applied on the inlet surface of the computational region:

$$v_w = v_{10}\left(z/10\right)^{0.2} \tag{6}$$

where v_{10} is the wind speed at the height of 10m. The details of the boundary conditions are shown in Table 2.

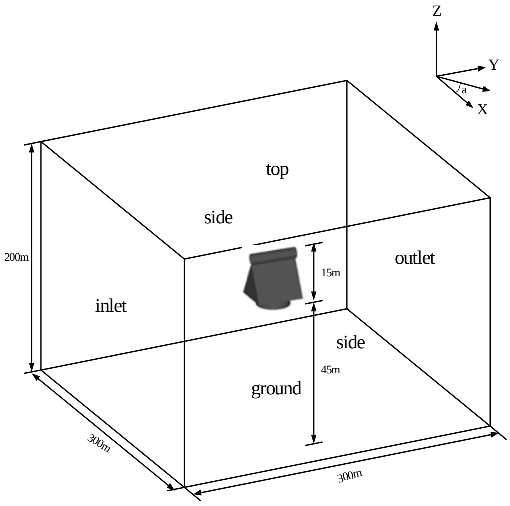

Fig. 4 Computational domain including the ACSC cell

Table 2 Details of the boundary conditions

Items	Boundary conditions
Wind-inlet	Velocity inlet (Figure.3)
Wind-outlet	Pressure outlet
Ground	Wall with air temperature
Side and top surface	Symmetry
Duct wall	Wall with exhaust temperature
Wind tube of the fan	Coupled wall
ACSC cell side surface	Coupled wall
Turbulence model	k-ε model
Wall function	Standard

3. INFLUENCE OF WIND SPEED ON THE PERFORMANCE OF ACSC CELL

The effect of the ambient conditions including wind speed, v_w, temperature, T_w, and direction angle, α, shown in Fig. 3, on the performance of the ACSC cell is investigated in the paper. It is assumed that the power plant operates at the turbine rating load (TRL) mode initially, and the exhaust steam parameters are shown in Table 3. The cell performance at TRL will be first simulated. Obviously, the ACSC working state will probably varies with the ambient condition, and the final stable state of the ACSC cell will also be forecasted.

Table 3 Steam parameters of the ACSC cell under TRL mode

Item	m_s (kg/s)	p_s (kPa)	α (%)	Δp_s (Pa)
value	6.59	29	96.4	820

The flow filed of the ACSC cell under different wind speeds is simulated when the wind direction is parallel to the steam duct, α=90, the wind temperature, T_w=306K. Volumetric effectiveness, e, the ratio between the actual fan flow rate to the ideal flow rate, is applied to characterize the influence of the wind speed on the fan performance. Here, the designed fan flow rate is assigned to the ideal flow rate, 467m^3/s.

The volumetric effectiveness and the frontal velocity drop obviously with the wind speeds in Fig. 5. They have the same trend because the volume flow rate divided by the frontal area of the exchanger is just the frontal velocity. The decrease amplitude reaches 20.7 percents when the wind speed rises from 0m/s to 10m/s.

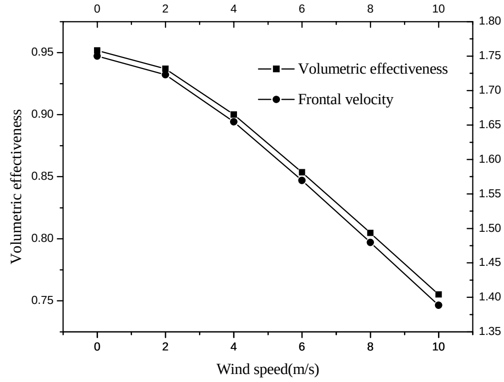

Fig. 5 Volumetric effectiveness and frontal velocity with wind speeds

Figure 6 shows the cross view of the static pressure around the ACSC cell at 0m/s and 10m/s. It can be seen that fan volumetric effectiveness is reduced due to an extending low-pressure region around the fan inlet. As a result, a larger power fan is demanded to guarantee the ACSC performance.

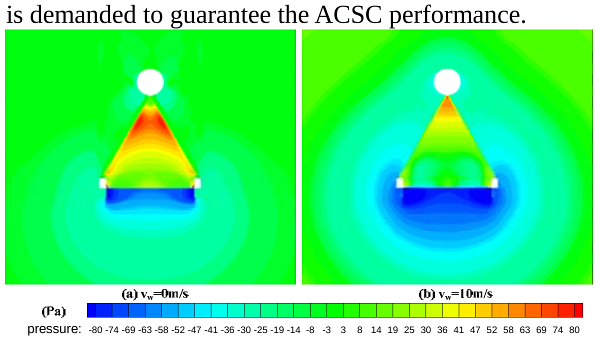

Fig. 6 Cross view of static pressure distribution under the effect of wind speed

The state of the turbine exhaust is unique if the steam pressure and quality are known in advance, and the pressure and quality are input into the UDF as the inlet parameters of the fluid grid in the exchanger. Enthalpy and pressure at the grid outlet are both calculated in sequence since the pressure loss is considered during steam condensation. Thus the heat transfer rate of exchangers in the ACSC cell is obtained from the sum of the grid release. The latent heat corresponding to each pressure during condensation is called the ideal heat release if the exhaust steam does not subcooled, and it can be expressed:

$$Q_{id} = m_s\left(h' - h''\right) \tag{7}$$

where Q_{id} is the ideal heat release, Q_{id}=14.88kJ/kg according to the TRL parameters; h' is the exhaust steam enthalpy, and h'' is the enthalpy of the saturated water.

Heat transfer rate between the ambient and the exhaust steam drops obviously with the increasing wind speed in Fig. 7. The intersection point implies that the ACSC cell can operate stable at TRL condition, and the control system will be activated to adjust the work state at other nonequilibrium points.

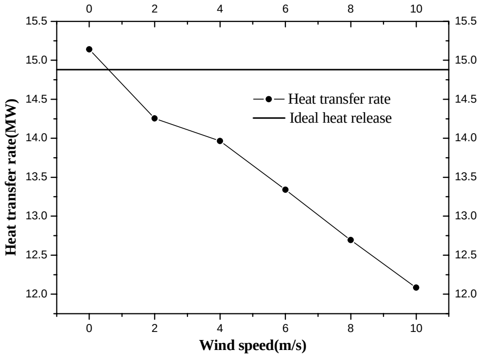

Fig. 7 Heat transfer rate with wind speeds

The trend of heat transfer rate with the wind speed can be explained in Fig. 8. The bottom temperature of the exchanger is almost equal to the wind temperature which implies the steam condensates completely or even subcools, and the heat transfer rate is larger than the ideal heat release. The exhaust temperature still appears at the exchanger bottom when the wind speed is 12m/s and the ideal heat release is not carried away completely by the environment. In fact, the reduction of the air volumetric effectiveness resulting from the wind speed directly causes the decreasing heat transfer rate.

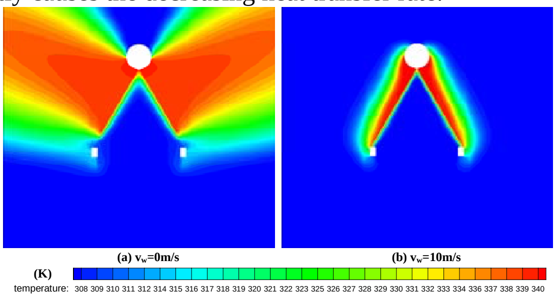

Fig. 8 Cross view of temperature distribution under the effect of wind speed

The ACSC cell operates instable at the selected wind speeds and the final back pressures of the cell corresponding to the wind speeds are numerically forecasted in Fig. 9. The back pressure rises from 27.9kPa to 60kPa with the increasing of the wind speed.

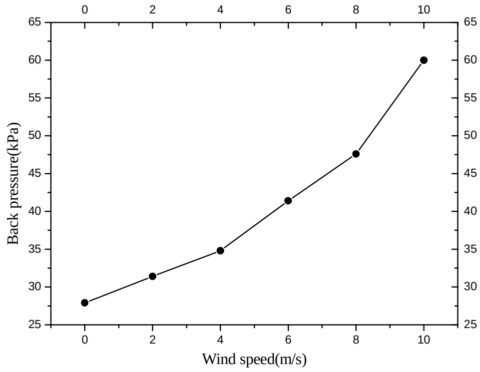

Fig. 9 Back pressure with wind speeds

The back pressure is finally forecasted in Table 4, and the ACSC cell will operate stable since the difference between the heat transfer rate and the ideal heat release is small enough to be ignored.

Table 4 Comparison between the heat transfer rate and the ideal heat release with wind speed

v_w(m/s)	0	2	4	6	8	10
p_s(kPa)	27.9	31.4	34.8	41.4	47.6	60
Q(MW)	14.90	14.83	14.79	14.73	14.68	14.59
Q_{id}(MW)	14.89	14.85	14.81	14.74	14.68	14.59

4. INFLUENCE OF WIND TEMPERATURE ON THE PERFORMANCE OF ACSC CELL

The ACSC performance is sensitive to the wind temperature because the temperature difference between the exhaust and environment indicates the potential heat transfer capacity of the heat exchanger. The performance of the ACSC cell under different wind temperatures is investigated, shown in Fig. 10, and the wind speed is 4m/s, the wind direction, α=90. Different from the effect of wind speed, the cold side temperature of the exchanger changes with the wind temperature, and then affects the heat exchanger performance. The back pressure increases from 17.8kPa to 34.8kPa when the wind temperature varies from 290K to 306K.

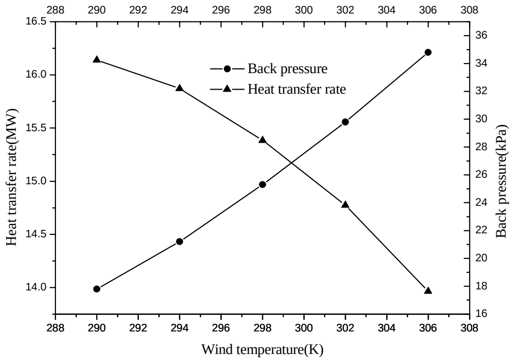

Fig. 10 Heat transfer rate and back pressure with wind temperature

Since the ideal heat release can be just carried away by the environment, shown in Table 5, the ACSC cell will operate stable at the corresponding back pressures.

Table 5 Comparison between the heat transfer rate and the ideal heat release with wind temperature

T_w(K)	290	294	298	302	306
p_s(kPa)	17.8	21.2	25.3	29.8	34.8
Q(MW)	15.06	15.01	14.95	14.88	14.79
Q_{id}(MW)	15.06	14.99	14.93	14.87	14.81

5. INFLUENCE OF WIND DIRECTION ON THE PERFORMANCE OF ACSC CELL

The influence of the wind direction on the ACSC cell performance is presented in Fig. 11 and Fig. 12, and the wind temperature is 306K, wind speed 4m/s. The range of 90 degree is investigated due to the symmetry of the numerical model. Similar to the effect of wind speeds, the volumetric effectiveness and frontal velocity are also sensitive to the wind directions because the flow field is different when the ambient wind blows from these direction angles. The effect trend of the wind direction is not monotonous. The results tells that the cross wind, α=0, is adverse for the fan performance. The volumetric effectiveness and frontal velocity are almost the same until α=30, and then rise with the increasing of the direction angle. But the back pressure reaches the peak value, 39kPa, at the adverse wind direction, α=30, and then drops again.

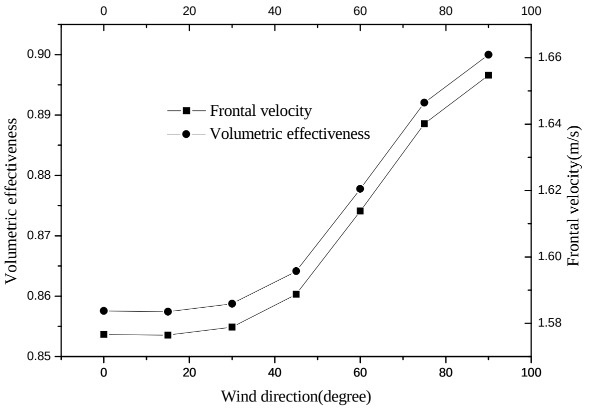

Fig. 11 Volumetric effectiveness and frontal velocity of the ACSC cell with wind direction

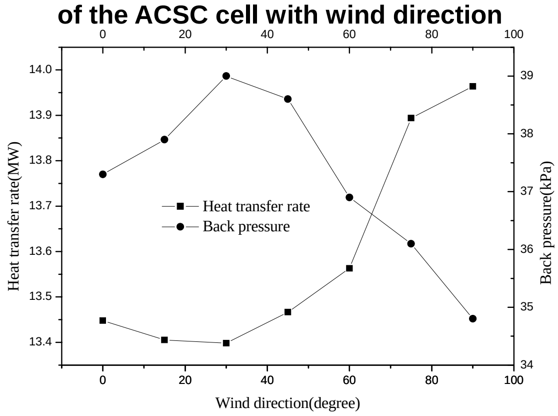

Fig. 12 Heat transfer rate and back pressure of the ACSC cell with wind direction

The ACSC cell can't operate at the initial assumed pressure according to the calculation results, and new pressures are obtained until the heat transfer rate is considered to be equal to the ideal heat release in Table 6.

Table 6 Comparison between the heat transfer rate and the ideal heat release with wind direction

α(degree)	0	15	30	45	60	75	90
p_s(kPa)	37.3	37.9	39	38.6	36.9	36.1	34.8
Q(MW)	14.76	14.79	14.78	14.76	14.77	14.79	14.79
Q_{id}(MW)	14.78	14.77	14.76	14.77	14.78	14.79	14.81

6. HOT AIR RECIRCULATION

Hot air recirculation (HAR), which implies hot air flow from the exchangers is drawn back into the fans, affects the performance of the ACSC cell because the inlet temperature of the exchangers is raised. Hot recirculation rate (HRR) is defined to characterize the impact extent of returning hot air:

$$C_R = \frac{T_f - T_w}{T_{out} - T_w} \tag{8}$$

where T_f is the average temperature of the fan inlet; T_{out} is the outlet temperature of the exchanger.

Wind wall, 10m in height, is equipped around the heat exchangers to prevent HAR and improve the performance of the ACSC cell. The HRR and cell performance with wind wall is compared with that of the original performance in Table 7. Here, the wind speed is 2m/s, and wind direction angle is 90 degree, wind temperature 306K.

Table 7 Comparison between the heat transfer rate and the ideal heat release with or without wind wall

Items	T_f (K)	C_R(%)	e	Q(MW)	p_s(kPa)
Original	309.9	11.03	0.94	14.25	31.4
Wind wall	306.2	0.03	0.91	14.89	29.0

Under the effect of the wind wall, T_f drops from 309.9K to 306.2K, and the corresponding HRR drops from 11.03% to 0.03%. The transform is well explained in the cross view of the streamline around the ACSC cell in Fig. 13. Hot air flow at the bottom of the exchangers where vortices appear is drawn back into the fan in Fig. 13(a), and the vortices mainly contribute to the raised fan inlet temperature and hot recirculation rate. But vortices move to the top of the wind wall, and the hot air is cooled before it flows into the fan in Fig. 13(b).

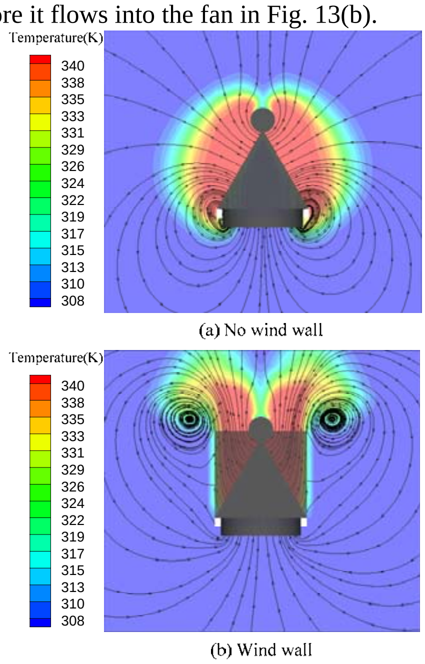

Fig. 13 Cross view of the streamline around the ACSC cell

Hot air recirculation is effectively suppressed after the wind wall is equipped around the heat exchangers, but the adverse effect exists simultaneously because a decrease of 3 percent of the volumetric effectiveness has occurred. Cross view of static pressure around the ACSC cell is presented in Fig. 14. Wind wall influences the normal outflow of the hot air from the exchangers because the hot air gathers between the wind wall and the exchangers. As a result, a high-pressure region appears in Fig. 14(b), and the pressure in the A-frame is also higher than the original condition. Fan performance is reduced corresponding to a lower volumetric effectiveness.

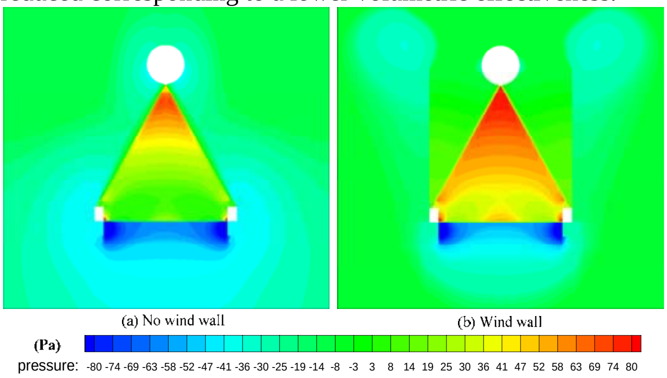

Fig. 14 Cross view of static pressure around the ACSC cell

Finally, the heat transfer rate rises and the back pressure is reduced significantly with the effect of wind wall in Table 7. It is inferred that the influence of hot air recirculation is more important on the performance of the ACSC cell. The original cell performance is optimized effectively through the wind wall.

7. CONCLUSIONS

A practical numerical model is proposed to simulate the flow field around the ACSC cell. The influence of the ambient conditions on the ACSC cell performance is numerically investigated, and the mechanism of the influence is demonstrated in the paper. In addition, the wind wall is equipped around the heat exchangers to prevent the hot air recirculation and raise the performance.

High wind speed and temperature both are adverse for the ACSC cell performance. High wind speed reduces the air flow rate participating in the heat transfer process between the ambient air and the exhaust steam while high wind temperature raises the exchanger inlet temperature. Similar to the effect of the wind speed, fan performance also varies under different wind directions. The peak back pressure is 39kPa at α=30 according to the simulation result.

The exchanger inlet temperature increases under the effect of hot air recirculation because the hot air is drawn back into the fan. The flow field around the ACSC cell changes under the effect of the equipped wind wall, and the hot recirculation rate is effectively suppressed. Finally, the cell performance is significantly improved although the volumetric effectiveness is reduced with gathering effect.

Nomenclature

Roman symbols	
a	steam quality
C	inertial resistance coefficient (m^{-1})
C_1, C_2, C_μ	constants in turbulence equations
C_R	hot air recirculation
e	volumetric effectiveness
h'	turbine exhaust enthalpy ($kJkg^{-1}$)
h''	saturated water enthalpy ($kJkg^{-1}$)
k	turbulent kinetic energy (m2s-2)
m	mass flow rate (kgs^{-1})
Δn	thickness of the exchangers (m)
p	pressure (pa)
Δp	pressure rise or pressure loss (pa)
P_r	Prandtl number
Q	heat transfer rate (MW)
S	source term (Nm^{-3})
t	time (s)
T	temperature (K)
v	velocity (ms^{-1})
x,y,z	coordinates (m)
Greek letters	
ρ	density (kgm^{-3})
μ	dynamic viscosity($kgm^{-1}s^{-1}$)
ε	Turbulent kinetic energy dissipation rate (m2s-3)
σ	Prandtl number for k, ε *and* T
Φ	general variable
Γ	diffusion coefficient
Subscripts	
e	exchanger
eff	effective
f	fan, frontal
id	ideal
n	normal
out	outlet
s	steam
t	turbulence
w	wind

REFERENCES

[1] Salta, C.A., Kroger, D.G., 1995. “Effect of inlet flow distortions on fan performance in forced draft air-cooled heat exchangers”. Heat Recovery Systems & CHP, 15(6), pp. 555-561.

[2] Stinnes, W.H., von Backstrom, T.W., 2002. “Effect of cross-flow on the performance of air-cooled heat exchanger fans”. Applied Thermal Engineering, 22(12), pp. 1403-1415.

[3] Hotchkiss, P.J., Meyer, C.J., von Backstrom, T.W., 2006. “Numerical investigation into the effect of cross-flow on the performance of axial flow fans in forced draught air-cooled heat exchangers”. Applied Thermal Engineering, 26(2-3), pp. 200-208.

[4] Thiart, G.D., von Backstrom, T.W., 1993. “Numerical simulation of the flow field near an axial flow fan operating under distorted inflow conditions”. Journal of Wind Engineering and Industrial Aerodynamics, 22(12), pp. 189-214.

[5] Meyer, C.J., Kroger, D.G., 2001. “Numerical simulation of the flow field in the vicinity of an axial flow fan”. International Journal for Numerical Methods in Fluids, 36(8), pp. 947-969.

[6] Duvenhage, K., Vermeulen, J.A., Meyer, C.J., et al, 1996. “Flow distortions at the fan inlet of forced-draught air-cooled heat exchangers”. Applied Thermal Engineering, 16(8-9), pp. 741-752.

[7] Bredell, J.R., Koger, D.G., Thiart, G.D., 2006. “Numerical investigation of fan performance in a forced draft air-cooled steam condenser”. Applied Thermal Engineering, 26(8-9), pp. 846-852.

[8] Meyer, C.J., 2005. “Numerical investigation of the effect of inlet flow distortions on forced draught air-cooled heat exchanger performance”. Applied Thermal Engineering, 25(11-12), pp. 1634-1649.

[9] Duvenhage, K., Kroger, D.G., 1996. “The influence of wind on the performance of forced draught air-cooled heat exchangers”. Journal of Wind Engineering and Industrial Aerodynamics, 62(2-3), pp. 259-277.

[10] Meyer, C.J., Kröger, D.G., 2001. “Air-cooled heat exchanger inlet flow losses”. Applied Thermal Engineering, 21(7), pp. 771-786.

[11] Meyer, C.J., Kroger, D.G., 1998. “Plenum chamber flow losses in forced draught air-cooled heat exchangers”. Applied Thermal Engineering, 18(9-10), pp. 875-893.

[12] Gao, X.F., Zhang, C.W., Wei, J.J., et al, 2009. “Numerical simulation of heat transfer performance of an air-cooled steam condenser in a thermal power plant”. Heat and Mass Transfer, 45(11), pp. 1423-133.

[13] Van Rooyen, J.A., Kroger, D.G., 2008. “Performance trends of an air-cooled steam condenser under windy conditions”. J. Eng. Gas Turbines Power, 130(023006), pp. 1-7.

[14] Owen, M.T.F., Kröger, D.G., 2010. “The effect of screens on air-cooled steam condenser performance under windy conditions”. Applied Thermal Engineering, 30(16), pp. 2610-2615.

[15] Gu, Z.F., Chen, X.R., William Lubitz, et al, 2007. “Wind tunnel simulation of exhaust recirculation in an air-cooling system at a large power plant”. International Journal of Thermal Sciences, 46(3), pp. 308-317.

[16] Liu, P.Q., Duan, H.S., Zhao, W.L., 2008. “Numerical investigation of hot air recirculation of air-cooled condensers at a large power plant”. Applied Thermal Engineering, 29(10), pp. 1927-1934.

[17] Jia, B.R., Yang, L.J., Du, X.Z., et al, 2009. “Influence of flow guiding device upon flow and heat transfer characteristics of air-cooled condenser cell”. Proceedings of the CSEE, 29(8), pp. 14-19.

[18] He, W.F., Dai, Y.P., Ma, Q.Z., et al, 2011. “Prediction of back pressure on the air-cooled unit with effect of ambient wind”. Journal of Xi’an Jiaotong University, 45(1), pp. 15-20.

[19] He, W.F., 2009. “Research on the influence of ambient wind speed to the operation performance of direct air-cooled power plant”. Master thesis, Xi’an Jiaotong University, Xi’an, China.